Compact localized boundary states in a quasi-1D electronic diamond-necklace chain

S. N. Kempkes,[1,*] P. Capiod,[2,3,*] S. Ismaili,[1] J. Mulkens,[2] I. Swart,[2,†] and C. Morais Smith[1,‡]

[1] *Institute for Theoretical Physics, Utrecht University, Netherlands*

[2] *Debye Institute for Nanomaterials Science, Utrecht University, Netherlands*

[3] *Junia-ISEN, Lille, France*

(Dated: January 7, 2022)

Abstract

Zero-energy modes localized at the ends of one-dimensional (1D) wires hold great potential as qubits for fault-tolerant quantum computing. However, all the candidates known to date exhibit a wave function that decays exponentially into the bulk and hybridizes with other nearby zero-modes, thus hampering their use for braiding operations. Here, we show that a quasi-1D diamond-necklace chain exhibits a completely unforeseen type of robust boundary state, namely compact localized zero-energy modes that do not decay into the bulk. We theoretically engineer a lattice geometry to access this mode, and experimentally realize it in an electronic quantum simulator setup. Our work provides a general route for the realization of robust and compact localized zero-energy modes that could potentially be braided without the drawbacks of hybridization.

* Both authors contributed equally.

† Correspondence to: i.swart@uu.nl

‡ Correspondence to: C.deMoraisSmith@uu.nl

Topological states of matter attracted a lot of interest in the previous years because of their potential use as qubits in a quantum computer[1–4]. These boundary localized states have an energy in the bulk gap and remain at that energy as long as the corresponding protecting symmetries are preserved. Since these modes are extremely robust against perturbations, the idea is that topological states can transfer information without loss into the environment.

One of the difficulties concerning quantum computing with topological states such as the non-Abelian Majorana bound states in a Kitaev chain[1,4,5] is their exponential decay into the bulk. When a Kitaev chain is too short, the quasiparticle Majorana-bound states at both edges hybridize and move away from zero energy. Therefore, in order to have a proper quantum computation, the length of the chain L should be long in comparison with the characteristic coherence length ξ, such that the amplitude of the exponentially decaying wave function $\propto \exp(-L/\xi)$ is small at the other side of the chain. Hybridization was experimentally shown to be an important factor in a quantum gate device[5]. This immediately brings stringent restrictions to the construction of a quantum gate based on topological states of matter.

Other possible candidates to store and transfer quantum information are *compact localized states*[6–15], which have until now been shown to exist in the *bulk*. These states correspond to eigenstates of the Hamiltonian that are completely localized in a certain sub-region of the lattice, and have strictly zero amplitude otherwise. Due to their local character, compact localized states are protected against perturbations outside the sites where they are located[13]. They occur in crystalline flat-band systems, where often frustration is causing the modes to be completely localized. As a result, these compact localized states do not mix with other bulk states and can be excited in a relatively easy manner, as shown experimentally in Refs.[10,11,16]. Furthermore, it has been recently proposed that these states could be used in a quantum network to transfer information in a proper and experimentally feasible manner[14]. Examples of these localized states can be found in (quasi)-1D lattices such as diamond, stub or cross chains, and in 2D, such as the Lieb lattice[7,8,10,11,15].

The compact localized states reported thus far occur in flat band systems, which means that these are bulk excitations and correspond to multiple degenerate modes. This can be beneficial when transferring information from one place to the other, but demands a large degree of control to excite a specific mode[10–12,16]. Furthermore, the proposal of transferring quantum information in a network requires a very controllable setup as well, which might be difficult to achieve in applications outside of a laboratory.

Here, we propose a very simple model, namely non-interacting electrons in a *quasi-1D diamond-necklace chain*, for which compact localized states occur at the *edges*. This chain bares some resemblance with the diamond chain, although in the latter the compact localized states are bulk modes[9,12,17]. The diamond-necklace chain has been studied in the context of spin chains[18–20], where it is known as the dimer-plaquette chain, and recently in the context of flat bands in a non-interacting lattice[21]. The end modes that we find are doubly degenerate, have an energy in the insulating bulk gap, are compactly localized at the extremities of the

lattice (no bulk decay), and are robust against a large number of perturbations. Furthermore, we show that the amplitude of the wave function of the zero mode can be fully controlled via either introducing anisotropies in the hopping amplitude or a flux in the plaquettes. We examine these compact states in an experimental setup and verify the theoretical proposal of compact localized end states in the diamond-necklace chain. These states open the path to the manipulation and braiding of boundary zero modes without the problem of hybridization of the end modes. Moreover, the 0D boundary modes in the SSH model have been proposed as building blocks for a poor man's quantum gate[22]. We expect similar properties for the end modes in this lattice, but with further protection.

The experimental setup that we use to verify the theoretical calculations is based on the electronic quantum simulator using CO adsorbed on a Cu(111) sample[23–26]. A Cu(111) substrate exhibits a 2D electron gas at its surface. The CO molecules act as repulsive scatterers for the surface electrons of the Cu(111) substrate, confining them to the area between the CO molecules[24,25,27,28]. This method and similar ones have been successfully used to fabricate flat-band models such as the Lieb lattice[25,29] and stub, diamond and cross lattices[15]. Further, these setups have been used to show robust zero modes in an SSH model[29], in a 2D kagome[28] and in a kekulé lattice[27]. However, in all these previous examples the corner modes decay exponentially into the bulk. The experimental results are compared with tight-binding and muffin-tin calculations, see Supplementary Information (SI) for further details. In the remainder, we first discuss the diamond-necklace chain in more detail and then describe the experiment.

The quasi-1D diamond-necklace lattice is shown in Fig. 1a. The lattice consists of 4 sites in a unit cell, connected with a hopping t_1. The Bloch Hamiltonian is given by

$$H(k) = \begin{pmatrix} \epsilon & -t_1 e^{-ik} & -t_1 & -t_1 \\ -t_1 e^{ik} & \epsilon & -t_1 & -t_1 \\ -t_1 & -t_1 & \epsilon & 0 \\ -t_1 & -t_1 & 0 & \epsilon \end{pmatrix}, \tag{1}$$

where k is the wave number and ϵ the onsite energy. Apart from three dispersive bands, the spectrum shows a flat band at energy $E = \epsilon$ corresponding to a wave function $|\psi\rangle = (0, 0, 1, -1)^T$, which is completely localized on the sites 3 and 4. The spectrum with $\epsilon = 0$ is shown in Fig. 1b. Now, we can open a gap in the spectrum by introducing a hopping $t_2 \neq t_1$ between sites 1-4 and 2-3, as shown in Figs. 1c-d. The localized state is no longer a solution to the Schrödinger equation and there is a gap at $E = \epsilon = 0$.

In a finite chain consisting of N sites, this band-gap opening gives rise to compact localized boundary states. The finite chain is shown in Fig. 1e; the chain starts and ends with a hopping t_3, which allows us to tune the amplitude of the localized wave functions. The spectrum of the finite chain as a function of t_2/t_1 is shown in Fig. 1f. In this finite chain, there is a zero-energy end mode, indicated in red in the spectrum. These states are

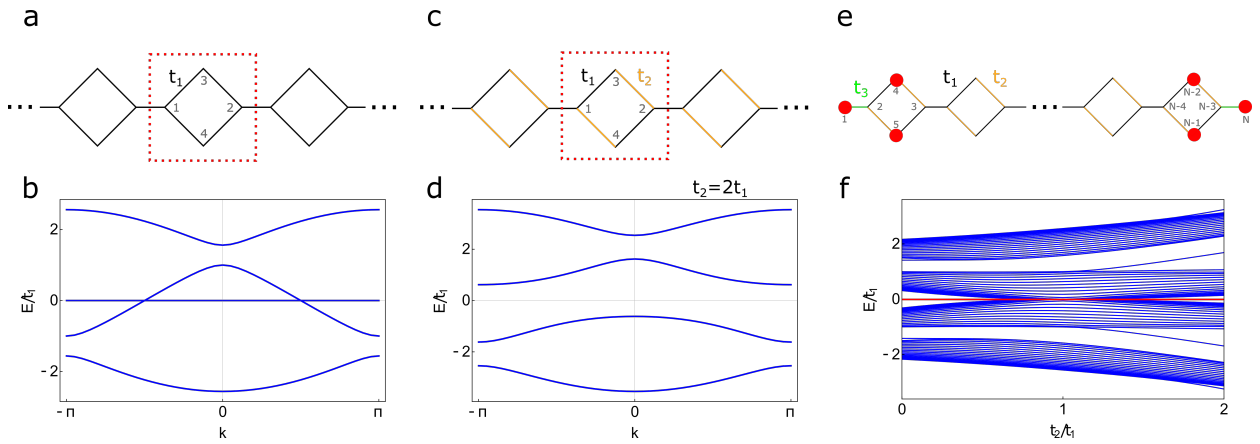

Figure 1. The quasi-1D diamond-necklace chain. **(a)** Periodic diamond-necklace chain with hopping t_1 connecting the four lattice sites (numbering indicated in grey). **(b)** Band structure for the lattice shown in (a). The band structure shows a flat band at $E = 0$. **(c)** The diamond-necklace lattice with the hopping t_2 between sites 1-4 and 2-3, and t_1 otherwise. **(d)** Band structure for the lattice show in (c) with $t_2 = 2t_1$. When $t_2 \neq t_1$, a band gap opens up at $E = 0$. **(e)** Finite-size lattice ending on both sides with a bond t_3. In this case, one can always find a degenerate state with $E = 0$ that is compactly localized at the boundaries of the chain when $t_2 \neq t_1$. The wave-functions amplitude of these wave functions are schematically shown in red and the exact amplitudes depend on the hopping parameters t_1, t_2 and t_3. **(f)** Spectrum of the finite-size lattice shown in (e) consisting of $N = 82$ sites and hopping parameters $t_3 = t_1$. The zero mode localized at the end of the chain is shown in red and is always compactly localized (no bulk decay) in the three lattice sites at the boundaries when $t_2 \neq t_1$.

compactly localized on sites 1, 4 and 5 on the left side of the chain and on sites $N-2$, $N-1$ and N on the right side of the chain when $t_1 \neq t_2$, as schematically shown with red disks in Fig. 1e. The modes can be understood as a hybrid of the compact localized bulk states in a diamond chain[9,12,30] and a boundary mode in the SSH model[31]. When considering the limit $t_3 = 0$, there are two isolated sites on either side of the chain, with a localized wave function at energy $E = \epsilon$. If $t_1 = t_2$, there are compact states in the bulk and the end mode can hybridize with the compact states near the boundary. When $t_1 \neq t_2$, there is a gap in the spectrum and therefore no state with the same energy in the bulk to hybridize with the edge mode. In this sense, one could expect an exponential decay from the end-localized states into the bulk if the hopping $t_3 \neq 0$, in a similar way as it occurs in the SSH model[31]. However, due to destructive interference, the zero mode does not decay exponentially into the bulk, but remains compactly localized at the edges.

We can write down an exact form of the wave function by making use of destructive interference[32–34]. In this perspective, we are looking for a (not-normalized) wave function of the form $|\psi\rangle = (1, 0, 0, r_1, r_2, 0, 0, ...)^T$ that has only an amplitude on the sites 1, 4 and 5 and

energy $E = \epsilon$. When acting on our trial wave function with the Hamiltonian corresponding to the finite chain, we find

$$H|\psi\rangle = \begin{pmatrix} \epsilon & -t_3 & 0 & 0 & 0 & 0 & \cdots \\ -t_3 & \epsilon & 0 & -t_1 & -t_2 & 0 & \cdots \\ 0 & 0 & \epsilon & -t_2 & -t_1 & -t_1 & \cdots \\ 0 & -t_1 & -t_2 & \epsilon & 0 & 0 & \cdots \\ 0 & -t_2 & -t_1 & 0 & \epsilon & 0 & \cdots \\ 0 & 0 & -t_1 & 0 & 0 & \epsilon & \cdots \\ \vdots & \vdots & \vdots & \vdots & \vdots & \vdots & \ddots \end{pmatrix} \begin{pmatrix} 1 \\ 0 \\ 0 \\ r_1 \\ r_2 \\ 0 \\ \vdots \end{pmatrix}$$

$$= \epsilon \begin{pmatrix} 1 \\ -(t_3 + t_1 r_1 + t_2 r_2)/\epsilon \\ -(t_2 r_1 + t_1 r_2)/\epsilon \\ r_1 \\ r_2 \\ 0 \\ \vdots \end{pmatrix}. \tag{2}$$

The wave function is a solution to the Schrödinger equation when $t_3 + t_1 r_1 + t_2 r_2 = 0$ and $t_2 r_1 + t_1 r_2 = 0$, which gives $r_1 = t_3 t_1/t$ and $r_2 = -t_3 t_2/t$, where $t = t_2^2 - t_1^2$. The eigenfunction with energy ϵ is then given by $|\psi\rangle = (1, 0, 0, t_3 t_1/t, -t_3 t_2/t, 0, 0, ...)^T$, and is completely localized. A similar calculation holds for the wave function localized on the right side of the chain. When $t_2 = t_1$, the amplitude on site 1 becomes zero and we obtain the compact localized state for the sites 4 and 5 corresponding to the states in the bulk flat band shown in Fig. 1b. Another way to open the bulk gap in the spectrum is to introduce a flux in the diamond part of the chain, as it was experimentally shown for a diamond chain[12]. By introducing a flux, we obtain the same physics for the compact localized boundary modes, but now the amplitude of sites 4 and 5 depends on the flux, see Supplementary Information (SI) for an explicit calculation.

Now, we examine some particular properties of these end modes. Since these modes are compactly localized, any perturbation outside of the boundary region will not disturb them. More generally, these modes are protected against any perturbation that does not couple to the sites 1, 4 and 5, and perturbations that preserve the destructive interference when connecting to sites 1, 4 and 5, see SI for further details. These features make the end modes robust against any kind of disorder in the bulk of the crystalline lattice. Furthermore, contrary to the exponentially decaying topological modes, this end-localized zero mode has no exponential decay into the bulk. This means that the wave functions of the end modes cannot hybridize with each other and gap out. Therefore, there are no finite-size effects hampering the protection of these end modes. Especially for quantum computations or braiding, the decay length of the topological boundary modes is one of the main issues that

can affect the performance[4]. Since there is no decay of the wave function in these compact localized modes, it is not possible to hybridize and the energy will remain strictly at zero. Finally, we note that the wave function amplitude at sites 1, 4 and 5 can be tuned at will. The amplitudes on site 4 and 5 only depend on the strength of the hopping parameters t_1, t_2, and t_3 at the boundaries, and are not influenced by variations of the parameters in the remainder of the chain. In the next section, we show how to experimentally engineer these boundary modes in an electronic lattice and how to change the wave function amplitude of the compact localized states by tuning the hopping t_3.

The theory presented in the previous section is now confronted with experiment. Figure 2 shows a constant-current image of a diamond-necklace chain realized by positioning CO molecules on a Cu(111) surface using the tip of an STM (Scienta Omicron LT-STM) operating at 4 K. Each CO molecule (black contrast) has been moved individually and is positioned using a procedure described in the literature[35–37]. The confined regions define atomic sites, see Fig. 2a. The boundary hopping t_3 is controlled by positioning the highlighted COs in Fig. 2a-c. In Fig. 2a, the highlighted CO molecules are far away from each other (1.28 nm), leading to a strong coupling between the neighboring sites (i.e. large t_3). In contrast, the highlighted COs are closer to each other (1.024 nm) in Fig. 2c, which decreases the boundary hopping amplitude t_3. The experimental spectra corresponding to the LDOS for the indicated sites from Fig. 2a-c are given in Fig. 2d-f (solid lines). Note that we only show the spectra on the left side of the chain, since the spectra on the right are similar by rotational symmetry. Spectra of additional sites are shown in the supporting information.
Upon inspection, we observe that the red spectrum (sites 1 and N, respectively) always has a peak-like structure around the onsite energy $V = -0.1$ V, whereas the bulk sites exhibit a gap-like structure around that energy (green site). Moreover, by positioning the highlighted CO molecules differently, one can change the LDOS of the blue site from exhibiting a peak (Fig. 2d) to having a dip (Fig. 2f) around $V = -0.1$ V. Hence, the amplitude of the wave function on that site can be modified via minor changes in the coupling strength t_3. The experimental observations are verified via a finite-size tight-binding calculation (dashed lines in Fig. 2d-f). In addition to the strong hopping parameter $t_1 = 0.095$ eV and the weak hopping $t_2 = 0.1t_1$ presented in Fig. 1e, we introduce the hopping $t_4 = 0.4t_1$ that connects the diamonds. To make the comparison with the experimental spectra, we only change the boundary hopping parameter t_3 from $0.8t_1$ (d), to $0.5t_1$ (e) and $0.3t_1$ (f) (and orbital overlap in a similar way, see SI). Also in the tight-binding LDOS, we clearly observe a large change in the blue spectra whereas the other spectra remain similar. Note that because of the coupling between the surface state with bulk states of the Cu crystal, the LDOS corresponding to the bulk sites of the chain does not completely vanish around $V = -0.1$ V. A comparison between the tight-binding and muffin-tin model is presented in the SI.
Next, we present wave-function maps of the created lattices with strong and weak coupling t_3 in Fig. 3. In Fig. 3a, we show the wave-function map for the strong boundary coupling chain at $V = -0.213$ V. At this energy, the electronic LDOS is mainly localized in the bulk

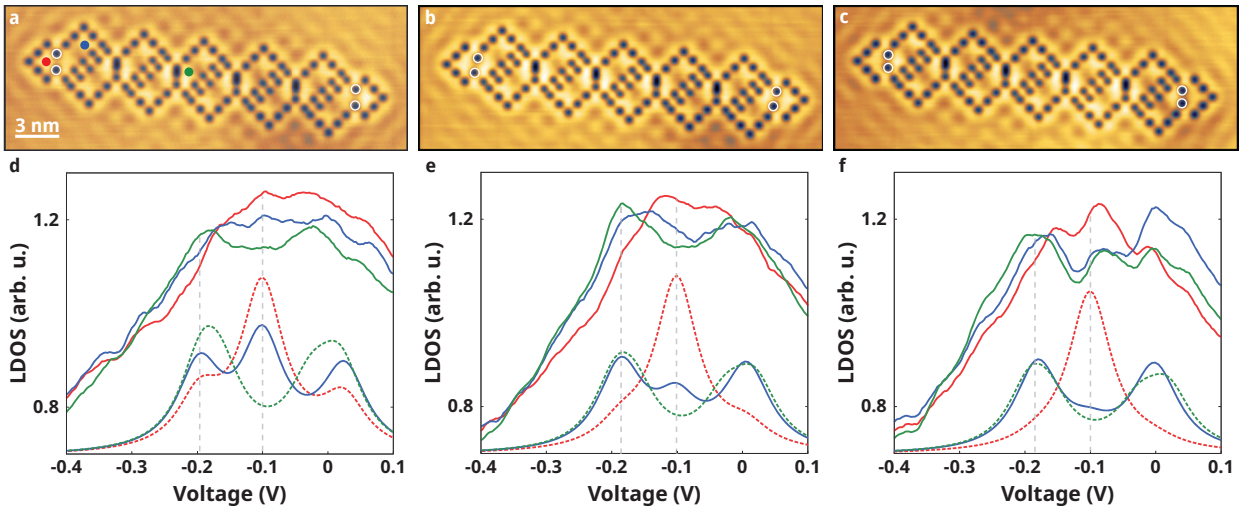

Figure 2. Experimental configuration and LDOS of the quasi-1D diamond-necklace chain **(a-c)** STM images of the diamond-necklace chain with a strong (a), intermediate (b) and weak (c) hopping t_3. The CO adsorbates are shown in black, of which four COs are highlighted. The highlighted COs determine the strength of the boundary hopping t_3. **(d-f)** Experimental spectra (solid lines) compared to the tight-binding spectra (dashed lines) of the sites indicated in (a). In the strong coupling (d), all spectra exhibit a gap around the onsite energy $V = -0.10\,\mathrm{V}$, except the spectra corresponding to the end sites (red and blue), which exhibit a peak. Upon decreasing the boundary hopping parameter t_3, we observe that the main difference in the spectra from the strong hopping (d) to the weak hopping (f) is the blue spectrum. When changing the COs near the edge of the lattice slightly, we influence the hopping parameter such that the spectrum on the blue site exhibits a peak around $V = -0.10\,\mathrm{V}$ for the strong hopping (d), and a dip around the same energy in the weak hopping regime (f). Here,$t_1 = 0.095\,\mathrm{eV}$, $t_2 = 0.1t_1$, and t_3 goes from $0.8t_1$ (d), to $0.5t_1$ (e) and $0.3t_1$ (f).

of the chain (bright colors), whereas it is absent in the end sites (dark colors), see Fig. 3a. When increasing the voltage to $V = -0.122\,\mathrm{V}$, the LDOS becomes more pronounced at the end modes of the lattice, more specifically on site 1 and 4, whereas the other sites and in particular site 2 show less intensity. A closer inspection of the end modes in the strong and weak chain is shown in Fig. 3c and d, respectively. We observe that the end mode is more pronounced on lattice site 4 with the strong boundary bonding t_3(Fig. 3c), and less pronounced in the weak boundary bonding t_3 (Fig. 3d). The tight-binding wave function amplitudes are represented as circles on top of the wave function map, where the circle radius scales linearly with $|\psi|^2$. The theoretical results indicate the same trend. A comparison in the framework of the muffin-tin model for these wave-function maps is shown in the SI.

To conclude, we have theoretically and experimentally introduced the notion of robust compact localized boundary states. These states are present in the insulating bulk-band gap and are completely localized at the boundary of the diamond-necklace chain. We have

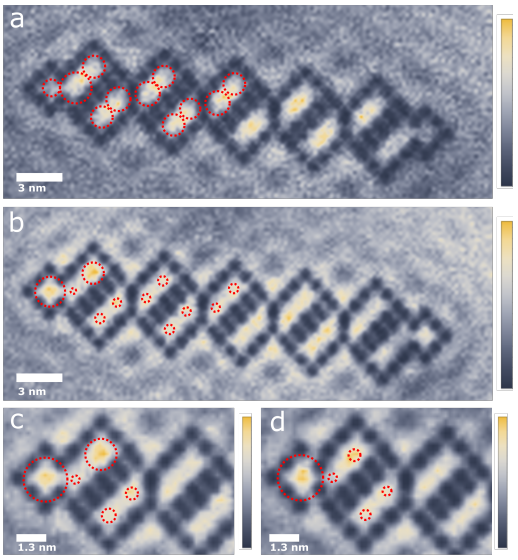

Figure 3. Experimental and tight-binding (red, dashed) wave-function maps of the boundary mode in the three chains. The circle radius of the tight-binding wave functions scales linearly with $|\psi|^2$ on the indicated site. **(a)** Wave-function map of the strong boundary hopping at $V = -0.213\,\mathrm{V}$. The wave function is localized in the bulk of the chain. **(b)** The wave-function map of the strong boundary hopping at $V = -0.122\,\mathrm{V}$. The amplitude of the wave function is now mainly localized at the ends of the chain. We note that due to imperfections in the determination of the sample tilt, the maps show deviations between the left and right sides of the chain. **(c-d)** Zoom in of the edge of the strong (c) and the weak (d) boundary hopping chain at $V = -0.122\,\mathrm{V}$. The relative weight of the wave function at site 1 increases upon decreasing the boundary hopping amplitude t_3, whereas the amplitude on site 3 decreases. This is in line with the observations from the tight-binding model.

shown how to change the wave-function amplitude of the boundary mode by controlling the boundary-hopping parameter, both in theory and in an experiment. Since these states are doubly degenerate and do not decay into the bulk, they might be the ideal candidates for quantum operations and to store and transfer information in the same way as the topological 0D modes in an SSH chain, with the difference that the chains do not need to be long in comparison with the decoherence length of the zero modes. It would be worthwhile to investigate whether compact Majorana bound-states can be realized in such a quasi-1D chain with the same non-Abelian properties as the ones in the Kitaev chain, and to perform braiding operations with those compact localized edge modes.

METHODS

Scanning tunneling microscopy experiments

The tunneling spectra in Fig. 2 were acquired at constant height, by placing the tip above a single site. The feedback loop is disconnected and a modulated voltage is applied to the tunneling junction. The tunneling current I and conductance dI/dV are measured simultaneously. The differential conductance is obtained with a lock-in amplifier (rms modulation of 10 mV at 769 Hz). All spectra were averaged using at least 18 dI/dV sets of reproducible curves. Density-of-state maps have been performed by disabling the feedback loop and activating the external voltage modulation of the lock-in. The energy has been carefully chosen from the LDOS curves (see Fig. 2), and the current has been set to 1 nA by adjusting the tip-surface distance.

Muffin-tin simulations

The experimental platform can be simulated by describing the surface state of the Cu(111) as a 2D electron gas that is patterned with circular potential barriers (CO molecules) with a height of V = 0.9 eV and a radius R = 0.3 nm[25]. We determine the energies and wave functions of this system by numerically solving the Schrödinger equation. To account for the coupling between the surface- and bulk states of copper, a Lorentzian broadening with a FWHM of 0.08 eV is applied to the theoretically computed energy levels.

ACKNOWLEDGEMENTS

We are grateful to M. di Liberto for discussions and D. Vanmaekelbergh for a careful reading of the manuscript. I.S. gratefully acknowledges financial support from the European Research Council (Horizon 2020 "FRACTAL", 865570).

---

[1] A. Y. Kitaev, Physics-Uspekhi **44**, 131 (2001).

[2] M. Z. Hasan and C. L. Kane, Reviews of Modern Physics **82**, 3045 (2010).

[3] X.-L. Qi and S.-C. Zhang, Reviews of Modern Physics **83**, 1057 (2011).

[4] V. Lahtinen and J. K. Pachos, SciPost Physics **3** (2017).

[5] S. M. Albrecht, A. P. Higginbotham, M. Madsen, F. Kuemmeth, T. S. Jespersen, J. Nygård, P. Krogstrup, and C. Marcus, Nature **531**, 206 (2016).

[6] B. Sutherland, Physical Review B **34**, 5208 (1986).

[7] S. Flach, D. Leykam, J. D. Bodyfelt, P. Matthies, and A. S. Desyatnikov, European Physics Letters **105**, 30001 (2014).

[8] W. Maimaiti, A. Andreanov, H. C. Park, O. Gendelman, and S. Flach, Physical Review B **95**, 115135 (2017).

[9] S. Mukherjee and R. R. Thomson, Optical Letters **40**, 5443 (2015).

[10] R. A. Vicencio, C. Cantillano, L. Morales-Inostroza, B. Real, C. Mejía-Cortés, S. Weimann, A. Szameit, and M. I. Molina, Physical Review Letters **114**, 245503 (2015).

[11] S. Mukherjee, A. Spracklen, D. Choudhury, N. Goldman, P. Öhberg, E. Andersson, and R. R. Thomson, Physical Review Letters **114**, 245504 (2015).

[12] S. Mukherjee, M. Di Liberto, P. Öhberg, R. R. Thomson, and N. Goldman, Physical Review Letters **121**, 075502 (2018).

[13] M. Röntgen, C. V. Morfonios, and P. Schmelcher, Physical Review B **97**, 035161 (2018).

[14] M. Röntgen, C. V. Morfonios, I. Brouzos, F. K. Diakonos, and P. Schmelcher, Physical Review Letters **123**, 080504 (2019).

[15] M. N. Huda, S. Kezilebieke, and P. Liljeroth, Phys. Rev. Research **2**, 043426 (2020).

[16] S. Xia, A. Ramachandran, S. Xia, D. Li, X. Liu, L. Tang, Y. Hu, D. Song, J. Xu, D. Leykam, S. Flach, and Z. Chen, Physical Review Letters **121**, 263902 (2018).

[17] J. Vidal, B. Douçot, R. Mosseri, and P. Butaud, Physical Review Letters **85**, 3906 (2000).

[18] J. Richter, N. Ivanov, and J. Schulenburg, Journal of Physics: Condensed Matter **10**, 3635 (1998).

[19] A. Koga, K. Okunishi, and N. Kawakami, Physical Review B **62**, 5558 (2000).

[20] J. Schulenburg and J. Richter, Physical Review B **65**, 054420 (2002).

[21] A. Nandy, Acta Physica Polonika A **40**, 164 (2019).

[22] P. Boross, J. K. Asbóth, G. Széchenyi, L. Oroszlány, and A. Pályi, Physical Review B **100**, 045414 (2019).

[23] M. F. Crommie, C. P. Lutz, and D. M. Eigler, Science **262**, 218 (1993).

[24] K. K. Gomes, W. Mar, W. Ko, F. Guinea, and H. C. Manoharan, Nature **483**, 306 (2012).

[25] M. R. Slot, T. S. Gardenier, P. H. Jacobse, G. C. van Miert, S. N. Kempkes, S. J. Zevenhuizen, C. M. Smith, D. Vanmaekelbergh, and I. Swart, Nature physics **13**, 672 (2017).

[26] A. A. Khajetoorians, D. Wegner, A. F. Otte, and I. Swart, Nature Reviews Physics , 1 (2019).

[27] S. E. Freeney, J. J. van den Broeke, A. J. J. H. van der Veen, I. Swart, and C. M. Smith, Physical Review Letters **124**, 236404 (2020).

[28] S. N. Kempkes, M. R. Slot, J. J. van den Broeke, P. Capiod, W. A. Benalcazar, D. Vanmaekelbergh, D. Bercioux, I. Swart, and C. Morais Smith, Nature Materials **18**, 1292 (2019).

[29] R. Drost, T. Ojanen, A. Harju, and P. Liljeroth, Nature Physics **13**, 668 (2017).

[30] M. Di Liberto, S. Mukherjee, and N. Goldman, Physical Review A **100**, 043829 (2019).

[31] W. P. Su, J. R. Schrieffer, and A. J. Heeger, Physical Review Letters **42**, 1698 (1979).

[32] F. K. Kunst, M. Trescher, and E. J. Bergholtz, Physical Review B **96**, 085443 (2017).

[33] F. K. Kunst, G. van Miert, and E. J. Bergholtz, Physical Review B **97**, 241405(R) (2018).

[34] F. K. Kunst, G. van Miert, and E. J. Bergholtz, Physical Review B **99**, 085426 (2019).

[35] L. Bartels, G. Meyer, and K.-H. Rieder, Physical Review Letters **79**, 697 (1997).

[36] G. Meyer, S. Zöphel, and K. H. Rieder, Applied Physics A **63**, 557 (1996).

[37] R. J. Celotta, S. B. Balakirsky, A. P. Fein, F. M. Hess, G. M. Rutter, and J. A. Stroscio, Review of Scientific Instruments **85**, 121301 (2014)

Supplementary Information

Compact localized boundary states in a quasi-1D electronic diamond-necklace chain

S. N. Kempkes, P. Capiod, S. Ismaili, J. Mulkens, I. Swart, and C. Morais Smith

In this supplementary information, we provide more details of the theoretical calculations presented in the main text. In particular, we discuss the opening of the band gap with a flux, the perturbations that are allowed to keep the boundary mode pinned at zero energy, and show a comparison between the muffin-tin and the tight-binding model.

THE DIAMOND-NECKLACE CHAIN

Flux in the diamond-necklace chain

In line with previous works on the quasi-1D diamond chain[S1,S2], we analyze what happens when a magnetic flux is piercing the diamonds in the lattice, see Fig. S1. The Bloch Hamiltonian

$$H(k) = \begin{pmatrix} \epsilon & te^{-ik} & -te^{i\varphi} & -t \\ -te^{ik} & \epsilon & -t & -t \\ -te^{-i\varphi} & -t & \epsilon & 0 \\ -t & t & 0 & \epsilon \end{pmatrix}, \tag{S1}$$

where t is the hopping amplitude, k the wave number, ϵ the onsite energy, and φ the flux per diamond. Introducing a nonzero flux in the diamond-necklace chain opens a band gap at $E = \epsilon = 0$ (Figs. S1a-d), similar to an anisotropic hopping, as was described in the main text. A π-flux gives rise to flat bands, in the same way as the Aharonov-Bohm cages do in the diamond chain[S1,S2], see Fig. S1d. In a finite-size lattice, a nonzero flux immediately gives rise to compact states as well. Using the same wave function as shown in the main text $|\psi\rangle = (1, 0, 0, r_1, r_2, 0, ...)^T$, we find in this case $r_1 = 1/[1 - \exp(i\varphi)]$ and $r_2 = -r_1$ for a compactly localized state, see Figs. S1e-f.

Perturbations

Next, we analyze which perturbations are allowed to keep the boundary mode localized and pinned to zero energy. Therefore, we observe what happens with the wave function when applying the general perturbations $a, b, c, d, ..., o$ (other perturbations are zero) in combination with different hopping parameters (t_1 to t_6, see Fig. S2). We find

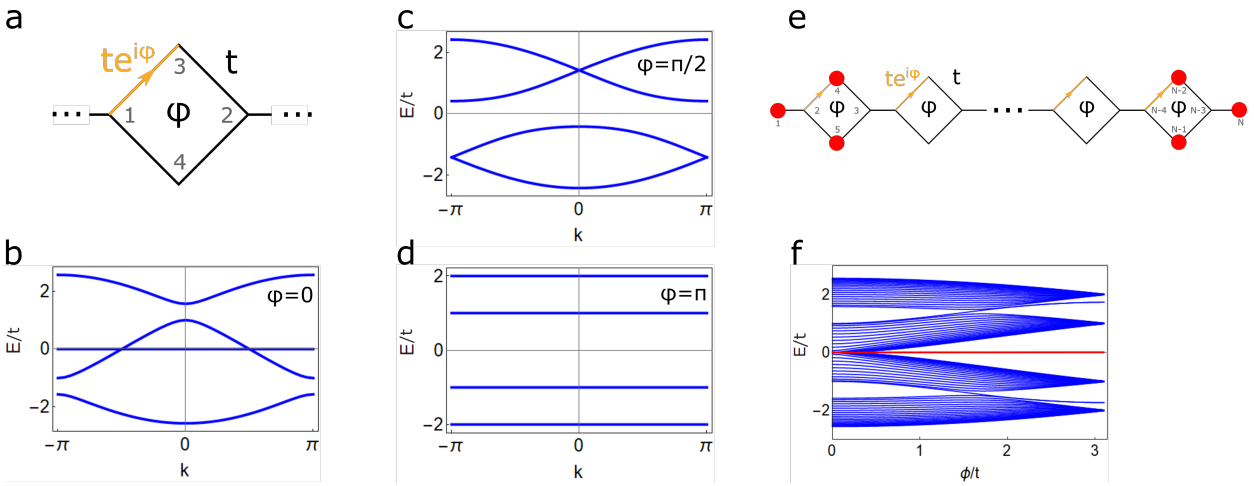

Figure S1. Flux in the diamond-necklace chain. (**a**) Unit cell of the diamond-necklace chain with hopping t and flux φ. (**b**) Band structure with $\varphi = 0$ and $\epsilon = 0$. (**c**) Band structure with $\varphi = \pi/2$. A gap opens up at $\epsilon = 0$. (**d**) Band structure with a π-flux. All the bands are completely flat. (**e**) Schematic of a finite-size lattice with a flux. The compact localized states are indicated by the red circles. (**f**) Band structure of the finite chain consisting of $N = 82$ sites. A nonzero flux opens up a gap at zero energy and gives rise to the compact localized states on sites 1, 4 and 5, and N-2, N-1 and N.

$$
H|\psi\rangle = \begin{pmatrix}
\epsilon & -t_1 & a & b & c & d & e & \cdots \\
-t_1 & \epsilon & f & -t_2 & -t_3 & g & h & \cdots \\
a & f & \epsilon & -t_4 & -t_5 & -t_6 & i & \cdots \\
b & -t_2 & -t_4 & \epsilon & j & k & l & \cdots \\
c & -t_3 & -t_5 & j & \epsilon & m & n & \cdots \\
d & g & -t_6 & k & m & \epsilon & o & \cdots \\
e & h & i & l & n & o & \epsilon & \cdots \\
\vdots & \vdots & \vdots & \vdots & \vdots & \vdots & \ddots &
\end{pmatrix}
\begin{pmatrix}
1 \\ 0 \\ 0 \\ r_1 \\ r_2 \\ 0 \\ 0 \\ 0 \\ \vdots
\end{pmatrix}
$$

$$
= \begin{pmatrix}
\epsilon + br_1 + cr_2 \\
-t_1 - t_2 r_1 - t_3 r_2 \\
a - t_4 r_1 - t_5 r_2 \\
b + \epsilon r_1 + j r_2 \\
c + j r_1 + \epsilon r_2 \\
d + k r_1 + m r_2 \\
e + l r_1 + n r_2 \\
\vdots
\end{pmatrix}. \tag{S2}
$$

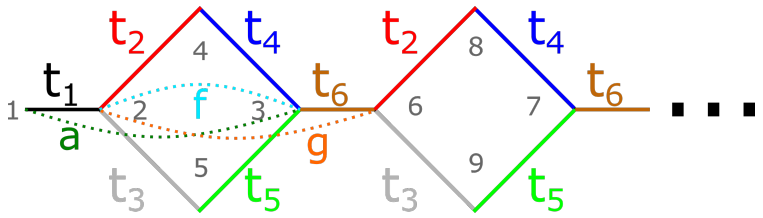

Figure S2. Schematic of the allowed perturbations a, f and g with general hopping parameters in the diamond-necklace chain (perturbations h and i are not included in this image to prevent clumping). Apart from these perturbations, any perturbation that preserves the destructive interference or does not couple to the sites 1, 4 and 5 is allowed.

From the latter expression, we observe that the wave-function amplitude on sites 1, 4 and 5 depends on these perturbing constants b, c, and j. To find the solution that obeys the Schrödinger equation with this eigenstate and energy ϵ, we need to solve 7 equations simultaneously (one for each line). There is no general solution for these equations. To simplify this, we set the constants that perturb the sites 1, 4 and 5 to zero, i.e. $b = c = j = 0$. Further, there is no general solution when the equations in the last two lines are present in the general form $d + kr_1 + mr_2$ and $e + lr_1 + nr_2$. For the moment, we also set those parameters d, k, m, e, l and n to zero, such that we have

$$
\begin{aligned}
H|\psi\rangle = &\begin{pmatrix}
\epsilon & -t_1 & a & 0 & 0 & 0 & 0 & \cdots \\
-t_1 & \epsilon & f & -t_2 & -t_3 & g & h & \cdots \\
a & f & \epsilon & -t_4 & -t_5 & -t_6 & i & \cdots \\
0 & -t_2 & -t_4 & \epsilon & 0 & 0 & 0 & \cdots \\
0 & -t_3 & -t_5 & 0 & \epsilon & 0 & 0 & \cdots \\
0 & g & -t_6 & 0 & 0 & \epsilon & o & \cdots \\
0 & h & i & 0 & 0 & o & \epsilon & \cdots \\
\vdots & \vdots & \vdots & \vdots & \vdots & \vdots & \ddots &
\end{pmatrix}
\begin{pmatrix}
1 \\ 0 \\ 0 \\ r_1 \\ r_2 \\ 0 \\ 0 \\ 0 \\ \vdots
\end{pmatrix} \\
= &\begin{pmatrix}
\epsilon \\
-t_1 - t_2 r_1 - t_3 r_2 \\
a - t_4 r_1 - t_5 r_2 \\
\epsilon r_1 \\
\epsilon r_2 \\
0 \\
0 \\
\vdots
\end{pmatrix}
= \epsilon
\begin{pmatrix}
1 \\ 0 \\ 0 \\ \frac{at_3 - t_1 t_5}{t_2 t_5 - t_3 t_4} \\ \frac{at_2 - t_1 t_4}{t_3 t_4 - t_2 t_5} \\ 0 \\ 0 \\ \vdots
\end{pmatrix},
\end{aligned}
\tag{S3}
$$

where the values for $r_1 = (at_3 - t_1 t_5)/(t_2 t_5 - t_3 t_4)$ and $r_2 = (at_2 - t_1 t_4)/(t_3 t_4 - t_2 t_5)$ were substituted into the last equation. In this way, we can find an analytic expression for the compact boundary states. These couplings and allowed perturbations a, f and g are

schematically shown in Fig. S2. We further note that other perturbations are allowed if the destructive interference is preserved. For example, we take line 6 in Eq. (S2): $d+kr_1+mr_2 = 0$. This line corresponds to connecting site 1, 4 and 5 to site 6. From the analysis of the perturbation, we know that $r_2/r_1 = -(at_2 - t_1t_4)/(at_3 - t_1t_5) = A$. When the constants are chosen such that $d = -(k+mA)r_1$, these perturbations will not affect the compact localized state. A similar analysis leads to $e = -(l+nA)r_1$ for the perturbation in line 7 of Eq. (S2), where sites 1, 4 and 5 are connected to site 7, and similar expressions follow in general for all sites connecting to the sites 1, 4, and 5. Furthermore, all perturbations that do not couple to the sites 1, 4 and 5 are allowed trivially. The same analysis can be done for the compact state localized on the right side of the chain. Therefore, we conclude that the end modes are robust against a large number of perturbations.

MUFFIN-TIN AND TIGHT-BINDING MODEL

We use the muffin-tin model to calculate the spectra for the configurations shown in Fig. 2. The wave-function maps for the bulk wave function at $E = -0.21\,\mathrm{eV}$ and the edge modes at $E = -0.14\,\mathrm{eV}$ are presented in Fig. S3. In these maps, we observe a shift in the amplitude for the boundary wave function to site 4 when the hopping parameter t_3 increases, whereas the bulk modes remain the same.

The results for the spectra of the same sites as in the main text are given in Figs. S4a-c for the strong (a), intermediate (b) and weak hopping (c) t_3. A Lorentzian broadening of $\Gamma = 80\,\mathrm{meV}$ is applied to the spectra to take the scattering with the bulk states into account. Further, we solve the finite-size tight-binding model with four hopping hopping parameters $t_1 - t_4$, as mentioned in the main text. Here, t_1 is the strong hopping within a diamond, t_2 is the weak hopping within a diamond, t_3 is the hopping to the boundary site and t_4 is the hopping connecting the diamonds. The parameters used in Figs. S4d-f are (all in eV): $e_s = -0.10$, $t_1 = 0.095$, $t_2 = 0.1t_1$, $t_4 = 0.4t_1$, and an NN orbital overlap of $s_1 = 0.1$, $s_2 = 0.1s_1$, $s_4 = 0.4s_1$. Further, the hopping parameters t_3 (overlap s_3) are $t_3 = 0.8t_1$ ($s_3 = 0.8s_1$) in Fig. S4d, $t_3 = 0.5t_1$ ($s_3 = 0.5s_1$) in Fig. S4e and $t_3 = 0.3t_1$ ($s_3 = 0.3s_1$) in Fig. S4f. The muffin-tin and tight-binding descriptions provide the same behavior as shown in Fig. S4.

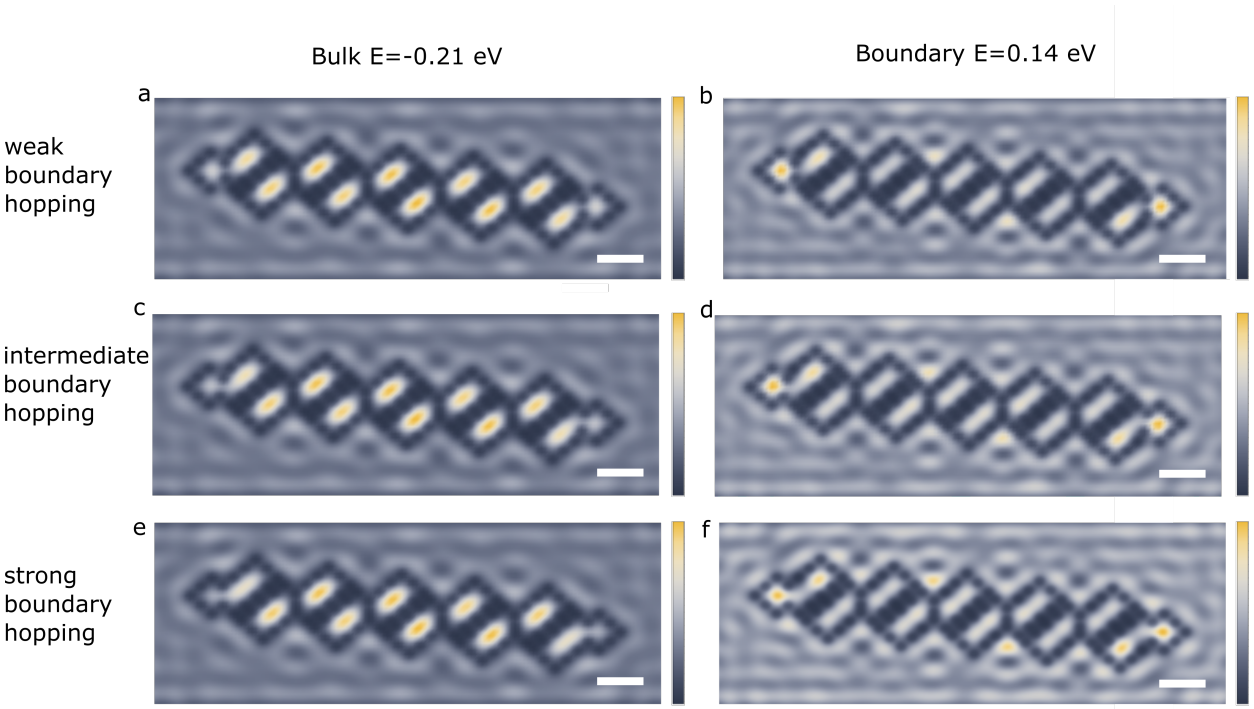

Figure S3. Wave function maps obtained from the muffin-tin model for the bulk and boundary modes. **(a-b)** Weak boundary hopping configuration. **(c-d)** Intermediate boundary hopping configuration. **(e-f)** Strong boundary hopping configuration. We observe a shift in amplitude for the boundary modes when going from weak to strong coupling. Scale bar 2.6 nm.

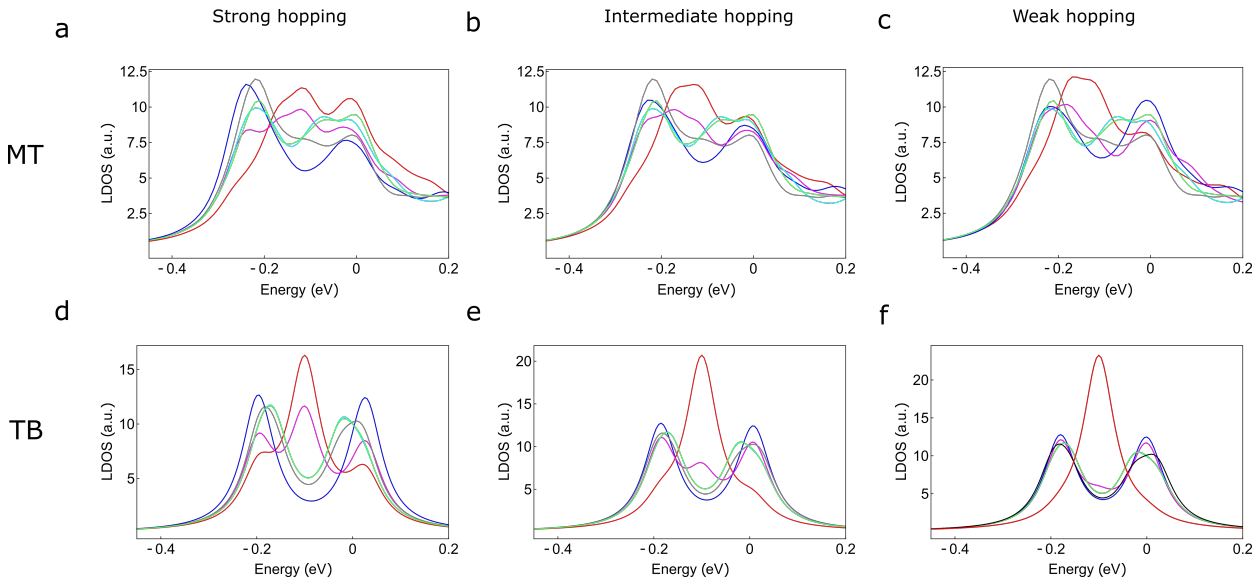

Figure S4. Comparison of the muffin-tin and tight-binding model. (**a-c**) LDOS of the sites in the strong (a), intermediate (b), and weak (c) hopping chain as indicated in the main text, obtained from the muffin-tin model. (**d-f**) LDOS of the sites in the strong (d), intermediate (e) and weak (f) hopping chain indicated in the main text obtained from the tight-binding model with the parameters indicated in the text. The similarity between the LDOS calculated using these two different methods is clearly visible.

ADDITIONAL DIFFERENTIAL CONDUCTANCE SPECTRA

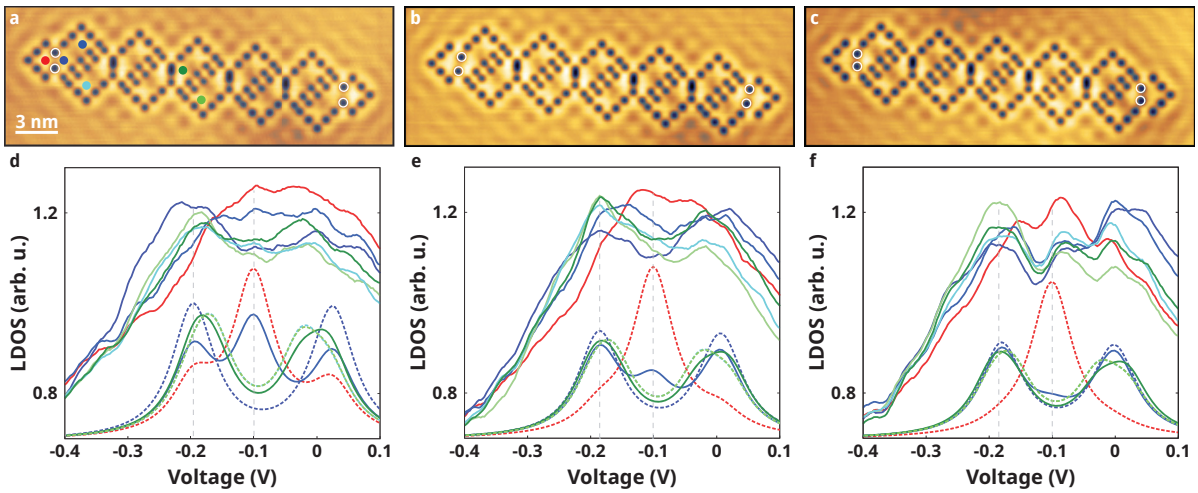

Figure S5. Differential conductance spectra of various sites and three configurations of the diamond-necklace chain. (**a-c**) LDOS of the sites in the strong (a), intermediate (b), and weak (c) hopping chain indicated in the main text, obtained from the muffin-tin model. (**d-f**) LDOS of the sites in the strong (d), intermediate (e) and weak (f) hopping chain indicated in the main text obtained from the tight-binding model with the parameters indicated in the text. The similarity between the LDOS calculated using these two different methods is clearly visible.

[S1] Mukherjee, S., Di Liberto, M., Öhberg, P., Thomson, R. R. & Goldman, N. Experimental Observation of Aharonov-Bohm Cages in Photonic Lattices. *Physical Review Letters* **121**, 075502 (2018).

[S2] Di Liberto, M., Mukherjee, S., & Goldman, N. Nonlinear dynamics of Aharonov-Bohm cages. *Physical Review A* **100**, 043829 (2019).